J. Biochem. 2012;151(5):483–492 doi:10.1093/jb/mvs028

JB THE JOURNAL OF BIOCHEMISTRY

A new structural insight into differential interaction of cyanobacterial and plant ferredoxins with nitrite reductase as revealed by NMR and X-ray crystallographic studies

Received December 10, 2011; accepted December 25, 2011; published online March 15, 2012

Yukiko Sakakibara[1,*], Hitoshi Kimura[2], Akira Iwamura[2], Takashi Saitoh[1], Takahisa Ikegami[1], Genji Kurisu[1,2] and Toshiharu Hase[1]

[1]Institute for Protein Research, Osaka University, 3-2 Yamadaoka, Suita, Osaka 565-0871; and [2]Department of Life Sciences, University of Tokyo, Komaba 3-8-1, Meguro-ku, Tokyo 153-8901, Japan

*Yukiko Sakakibara, Institute for Protein Research, Osaka University, 3-2 Yamadaoka, Suita, Osaka 565-0871, Japan. Tel: +81-(0)6-6879-8611, Fax: +81-(0)6-6879-8613, email: enzyme@protein.osaka-u.ac.jp

The atomic coordinates and structure factors (code 3B2F and 3B2G) have been deposited in the Protein Data Bank Japan, a member of the worldwide PDB (http://www.pbbj.org/).

Ferredoxin (Fd), which plays a pivotal role in photosynthesis as an electron carrier, forms a transient complex with various Fd-dependent enzymes, such as nitrite reductase (NiR), to achieve efficient intermolecular electron transfer. We studied the protein–protein interaction of Fd and NiR by NMR spectroscopy and determined three acidic regions of Fd to be major sites for the interaction with NiR, indicating that the complex is stabilized through electrostatic interaction. During this study, we found Fds from higher plant and cyanobacterium, in spite of their high structural similarities including the above acidic regions, differ remarkably in the interaction with cyanobacterial NiR. In activity assay of NiR, K_m value for maize Fd (74.6 μM) was 9.6 times larger than that for *Leptolyngbya boryana* Fd (7.8 μM). The two Fds also showed a similar difference in binding assay to NiR-immobilized resin. Comparative site-specific mutagenesis of two Fds revealed that their discriminative ability for the interaction with NiR is attributed mainly to non-charged residues in the peripheral region of [2Fe–2S] cluster. These non-charged residues are conserved separately between Fds of plant and cyanobacterial origins. Our data highlight that intermolecular force(s) other than electrostatic attraction is(are) also crucial for the molecular interaction between Fd and partner enzyme.

Keywords: Ferredoxin/nitrite reductase/protein–protein interaction/electron transfer.

Abbreviation: Fd, ferredoxin; FdI, leaf ferredoxin I; FNR, Fd-NADP$^+$ reductase; FTR, sFerredoxin–thioredoxin reductase; HSQC, heteronuclear single-quantum correlation; LbFd, *Leptolyngbya boryana* ferredoxin; NiR, nitrite reductase; NMR, nuclear magnetic resonance; RMSD, root mean square deviations; SiR, sulphite reductase; WT, wild-type.

Ferredoxin (Fd) is an acidic, iron–sulphur protein with a molecular mass of ~11 kDa and plays an important role as an electron carrier in a multitude of redox reactions in cyanobacteria and chloroplasts of photosynthetic eukaryotes. The midpoint potential (E_m) of [2Fe–2S] cluster of Fds from various organisms is very low with a range from −390 to −425 mV (*1*), and negatively charged residues are mainly distributed throughout the molecular surface on the side of [2Fe–2S] cluster (*2–6*). It has been shown by a variety of techniques that Fd forms electrostatically stabilized complexes with various Fd-dependent enzymes, such as Fd-NADP$^+$ reductase (FNR), sulphite reductase (SiR), nitrite reductase (NiR), glutamate synthase and Fd–thioredoxin reductase (FTR) for efficient intermolecular electron transfer (*7*).

Crystal structures of complexes between Fd and partner enzymes, maize leaf Fd/FNR, *Anabaena* Fd/FNR and *Synechocystis* Fd/FTR, have been determined (*2*, *5*, *8*). A set of positively charged residues of the partner enzymes is close to the acidic residues of Fd in a spatially matching manner to form salt bridges. The interaction sites of Fd with FNR, SiR and FTR were also elucidated in solution state by NMR chemical shift perturbation and cross saturation experiments (*9*, *10*). Combined data demonstrate that although a narrow Fd-binding site exists around positively charged cleft of Fd-dependent enzymes in common, molecular shapes of the sites differ considerably. Thus, Fd is bound to partner enzymes through a part of its whole acidic surface and such region seems to be at least partly unique for each of partner enzymes. This topological variety of the molecular recognition between Fd and partner enzymes would be significant for physiological function of Fd as a hub protein to distribute photosynthetic reducing power to a network of redox metabolisms occurring in one cellular compartment (*11*, *12*). We have been focusing on NiR to obtain further knowledge on the structural basis for the multi-functionality of Fd, because NiR utilizes the majority of reducing power in the metabolic network, and because structural information on the complex formation of Fd and NiR is limited.

NiR, which is a soluble monomeric protein with a molecular mass of 50–65 kDa, catalyses the six-electron reduction of nitrite to ammonia (*7*). In common with other Fd-dependent enzymes, NiR forms a 1:1 complex with Fd (*13*). The enzyme carries [4Fe–4S] cluster and sirohaem. By EPR and Raman spectroscopic studies a mechanism of nitrite reduction was proposed (*14–16*). E_m of [4Fe–4S] cluster and sirohaem of spinach NiR is −365 and −290 mV, respectively (*16*). This suggests that [4Fe–4S] cluster of NiR principally accepts one electron from [2Fe–2S] cluster of Fd, and subsequently transfers it to sirohaem. The crystal structure of spinach NiR (*17*) showed the prosthetic groups are buried within a hydrophobic cleft formed with three domains of NiR polypeptide. Positively charged residues are localized around the cleft and a sequence alignment of NiRs from various species reveals that most of these positively charged residues are conserved (*18*). Mutation of some of the charged residues led to decrease the interaction with Fd (*19*).

In this work, we have studied interaction of cyanobacterial NiR and two evolutionally divergent Fds from maize and cyanobacteria. Both Fds had comparable activity as an electron donor to NiR, but, interestingly, cyanobacterial Fd showed about 10 times stronger affinity with NiR than plant Fd. The crystal structures of both Fds were determined and their interactions with NiR were studied by 2D NMR spectroscopy. The results showed that the electrostatic interaction stabilizes the Fd/NiR complex in both cases. We considered that a subtle difference in the surface structure formed by non-charged residues would be the major factor for the differential affinity of two Fds with NiR. We have further verified this hypothesis by site-directed mutagenesis.

Materials and Methods

Site-directed mutagenesis and purification of Fds

Fd from *Leptolyngbya boryana* (formally *Plectonema boryanum*) (LbFd) (*20*) and maize leaf Fd isoprotein I (FdI) (*21*, *22*) were prepared as a recombinant protein expressed in *Escherichia coli* JM109 essentially as described previously. Site-specific mutants of LbFd and FdI were generated with QuikChange site directed mutagenesis kit (Stratagene). The list of mutants generated in this study and synthetic oligonucleotides used for the mutagenesis is shown in Supplementary Table S1. The mutation sites and the sequence integrity of the entire coding regions of mutant Fds were confirmed by nucleotide sequencing. [^{15}N,^{13}C]LbFd, [^{15}N]LbFd and [^{15}N]FdI were prepared essentially as described previously (*9*).

Expression and purification of Synechocystis sp. 6803 NiR

Coding region of *Synechocystis* sp. 6803 NiR was amplified by PCR using its genomic DNA as a template with the following primers, 5′-GGC CTC ATG ACT AAT AAA TTT GAG ACC GTT AAG GCA ACC and 3′-CCC GAG CTC AAC GCC GCA CAG CGC CAA ATT G, which contained BspHI and SacI, respectively. The PCR products were digested with BspHI and SacI and ligated into pTrc99A which had been digested with NcoI and SacI. As NiR needs to assemble with sirohaem to be the holoenzyme, sirohaem synthase gene (Cys G) from *E. coli*, which has EcoRV and HindIII at the 5′- and 3′-ends, respectively, was also introduced into the SmaI and HindIII sites of pTrc99A. This pTrc99A derived plasmid harbouring NiR and CysG genes was used for recombinant expression in *E. coli* JM109. Bacterial cells were grown in LB medium at 27°C for 3 h with vigorous aeration. IPTG was added to a final concentration of 100 μM when its absorbance at 600 nm reached to 0.5–0.6. The bacterial cells were harvested after further growth for 16 h.

The bacterial cells were suspended in 50 mM Tris–HCl, pH 7.5, 200 mM NaCl, 1 mM $MgCl_2$, 1 mM EDTA, 0.1% (v/v) 2-mercaptoethernol and 0.5 mM PMSF, disrupted by sonication and centrifuged at 10,000*g* for 15 min. The resulting supernatant was mixed with DEAE–cellulose (DE52, Whatman) in a batch-wise manner. The pass-through fraction containing NiR was fractionated with ammonium sulphate precipitation between 30% and 65% saturation. Crude NiR was desalted though a Sephadex G-25 column equilibrated with 50 mM Tris–HCl, pH 7.5, applied to an anion-exchange column (Resource-Q, GE Healthcare), and eluted with a linear gradient from 0 M to 0.5 M NaCl in 50 mM Tris–HCl, pH 7.5. Fractions containing NiR were combined, added with ammonium sulphate to a concentration of 40% and applied onto a Phenyl Sepharose column (GE Healthcare). NiR was eluted with a linear gradient from 40% to 0% ammonia sulphate in 50 mM Tris–HCl, pH 7.5. NiR was further purified by affinity chromatography on a column of LbFd-immobilized Sepharose-4B prepared as described previously (*9*). The final preparation of NiR showed absorption spectrum with maxima at wavelength of 278, 386 and 571 nm and a single band on SDS–polyacrylamide gel electrophoresis (Supplementary Fig. S1). This absorption spectrum was essentially the same as those reported for NiR from other organisms (*23*). Concentration of NiR was determined using an extinction coefficient of 18 000 M^{-1} cm^{-1} at 572 nm.

Assay of NiR activity

Fd-dependent NiR activity was measured in 50 mM Tris–HCl, pH 7.5 containing certain concentration of NaCl. The reaction was carried out in 0.5 ml reaction mixture, which contained 1 mM $NaNO_2$, 0.5 mM NADPH, 10 nM NiR, 0.1 μM FNR and various concentration of Fds (0–60 μM). An NADPH-generating system of 5 mM Glc-6-P and one unit Glc-6-P dehydrogenase was supplemented in the mixture. The reaction was initiated by adding NADPH and carried out at 25°C, and 50 μl aliquot of the mixture was taken for diazo coupling reaction of nitrite at 5 min intervals for 30 min (*24*). The diazo compounds standardized with nitrite were measured at 543 nm.

Structure determination and crystallographic refinement of Fds

LbFd and FdI dissolved in 50 mM Tris–HCl, pH7.5 containing 100 mM NaCl were concentrated to 15 mg/ml and 40 mg/ml, respectively. Crystallization conditions of two Fds were searched by the hanging drop vapour diffusion method. Crystals of LbFd were obtained at 20°C using 2.2 M ammonium sulphate in 100 mM sodium citrate, pH 5.2 as a reservoir solution. Crystals of FdI were obtained at 4°C from equal volumes of the protein solution and the reservoir solution (2.9 M ammonium sulphate in 100 mM sodium citrate, pH 5.5 containing 0.2% benzamidine). Diffraction images were collected at liquid nitrogen temperature (100 K) on CCD-based and imaging-plate detector systems. Details of the X-ray data collection are shown in Supplementary Table S2. The structures of LbFd and FdI were solved by molecular replacement method with the program MOLREP (*25*) using *Spirulina platensis* Fd structure (PDB ID: 4FXC) and *Equisetum arvense* FdI structure (PDB ID: 1FRR) as a search model, respectively. Manual revision of the atomic model was carried out with the program coot (*26*). Subsequent refinement was carried out up to 1.70 Å resolution for LbFdI and 1.70 Å resolution for FdI. The stereo-chemical geometry of two models was checked with the program PROCHECK (*27*). Structural images were prepared and superimposed using the program PyMOL (Delano Scientific). The sequences of LbFd and FdI were aligned using CLUSTAL-W (*28*). Surface potentials were generated using Poisson–Boltzmann electrostatic calculation methods (PDB2PQR and ABPS input) (*29*) with spinach stromal medium conditions (*30*).

NMR experiment and resonance assignment

The backbone assignments of LbFd were performed using 2D ^{1}H–^{15}N HSQC, 3D CBCA(CO)NH, HNCACB and HN(CO)CA at 293 K on a Bruker DRX-500 spectrometer (*31*). The NMR data were processed with NMRPipe (*32*) and analysed with Sparky (*33*) (Supplementary Table S3). For chemical shift perturbation experiments, [^{15}N]Fds mixed with increasing quantities of non-labelled NiR at molar ratios (NiR/Fd) of 0, 0.25, 0.5, 0.75, 1, 1.25 and 1.5 were recorded at 298 K on a Bruker AV-400M spectrometer.

Weighted averages of the ^{1}H ($\Delta\delta^{1}HN$) and ^{15}N ($\Delta\delta^{15}N$) chemical shift changes (ppm) were calculated with an equation of $\{[(\Delta\delta^{1}HN)^{2}+(0.17\times\Delta\delta^{15}N)^{2}]^{1/2}\}$, where 0.17 was calculated on the basis of the ratio between the chemical shift distributions of ^{1}H and ^{15}N spins in the amide groups of general folded proteins in terms of the respective ppm units. Thus, the value functions as the normalization factor that balances the difference between the ^{1}H and ^{15}N chemical shift changes (*9*).

Root mean square deviation calculation

The specified Cα atoms of LbFd (residues 1–10, 12–14 and 16–98) and FdI (residues 1–96) were superimposed and root-mean square deviations (RMSDs) of the main-chain and side-chains were calculated using the lsqkab programme in CCP4 (Supplementary Fig. S3) (*34*).

Results

Cyanobacterial and plant Fds differ in their protein–protein interaction with NiR

The Fd-dependent activity of NiR driven by LbFd or FdI was measured (Fig. 1A). Kinetic analysis revealed that although the maximum velocity was comparable between two Fds, the K_m value of NiR for LbFd (7.8 μM) was lower than that for FdI (74.6 μM). As the complex of NiR and Fd is considered to be stabilized mainly by electrostatic interaction, we investigated how NaCl added to the assay mixture influences NiR activity driven by two Fds (Fig. 1B). LbFd showed an activity profile with the maximum value in the presence of 50–100 mM NaCl followed by a gradual decline under higher NaCl concentrations. We consider that the complex formation of LbFd and NiR optimal for the intermolecular electron transfer could be achieved in the presence of a low concentration of the salt. FdI showed no such profile and a greater drop in activity than LbFd with increasing NaCl concentrations, indicative of a weaker affinity of FdI with NiR. Interaction of these Fds with NiR was further examined by affinity chromatography on a column of NiR-immobilized resin. FdI eluted at lower NaCl concentration than LbFd (Fig. 1C). These combined data indicate that the protein–protein interaction of NiR with cyanobacterial Fd was significantly stronger than that with higher plant Fd. A complex formation of NiR and two Fds was also investigated by gel-filtration chromatography to confirm this conclusion (Supplementary Fig. S2).

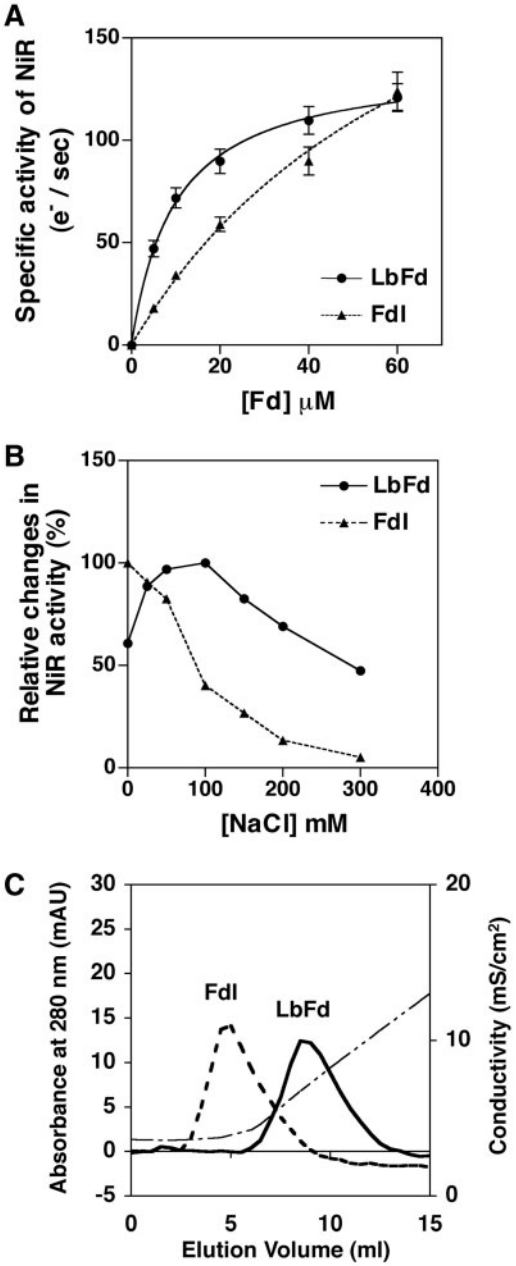

Fig. 1 NiR activity and binding assay of LbFd and FdI. (A) Fd-dependent activity of NiR was measured in 50 mM Tris–HCl, pH 7.5, containing 50 mM NaCl at 25°C. Fd was added in the assay mixture with increasing concentrations from 0 to 60 μM. The data obtained from three measurements were fitted by non-linear regression using Michaelis–Menten equation. (B) Fd-dependent activity of NiR was measured as in (A) in the presence of increasing concentrations of NaCl from 0 to 300 mM. (C) Fd was chromatographed on an NiR-immobilized Sepharose column with a linear gradient of NaCl from 0 to 0.5 M in 50 mM Tris–HCl, pH 7.5.

The X-ray crystallographic analysis of FdI and LbFd

To explore the differential characteristics of two Fds, we determined their X-ray crystal structures. Refined models of LbFd and FdI contained two Fd molecules in the asymmetric unit. The final crystallographic *R* factors and free *R* factors were 17.26% and 24.38% for LbFd at 1.76 Å resolution, and 22.45% and 28.81% for FdI at 1.70 Å resolution, respectively. All amino acid residues of LbFd and FdI except glycine and proline residues were in the stereo-chemically allowed regions in the Ramachandran plot. Refinement statistics are summarized in Supplementary Table S2.

Comparison of the crystal structures of LbFd and FdI showed a high similarity in their overall structures (Fig. 2A), as expected from a high-sequence homology of two Fds (64% identity) (Fig. 2B). Conserved amino acids are mainly distributed on the side where [2Fe–2S] cluster is located, whereas most of the non-conserved residues exist on the opposite side (Fig. 2C). Negatively charged areas are found at the periphery of [2Fe–2S] cluster region (Fig. 2D). Several distinctive features are also seen: (i) LbFd has an insertion of two amino acid residues at positions 10 and 14, forming a loop structure longer than that of FdI and (ii) The addition of two residues in the C-terminus of FdI

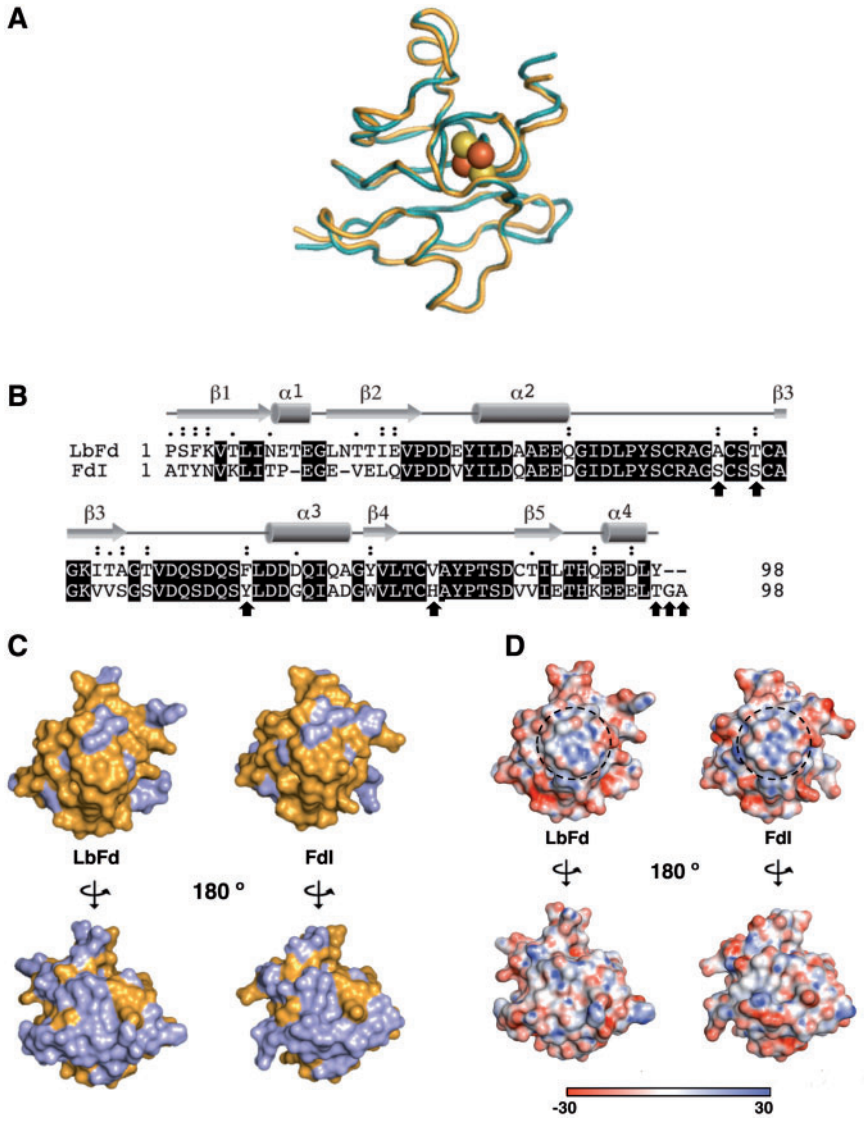

Fig. 2 Structural comparison of LbFd and FdI. (A) Superposition of the 3D structures of LbFd (blue) and FdI (yellow). The iron–sulphur cluster is shown as spheres. (B) Sequence alignment of LbFd and FdI with their secondary structures. White letters on black show identical residues between two Fds, and double and single dots show conserved and semi-conserved residues. Substituted residues in Fig. 6 were marked by arrows. (C) Identical and different residues between two Fds are coloured in yellow and grey, respectively, on the 3D structures of LbFd and FdI. (D) Electrostatic surface potentials of LbFd and FdI. Positive potential is shown in blue and negative potential in red. [2Fe–2S] cluster is located at the inner surface of the area circled with black dashed line.

forms a long helix structure. These distinctive futures are conserved in most of cyanobacterial and higher plant Fds (data not shown).

Identification of LbFd residues involved in complex formation with NiR

To obtain direct information about the protein–protein interaction of LbFd with NiR, we measured $^{1}H–^{15}N$ HSQC spectra of [^{15}N]LbFd and analysed chemical shift perturbations of LbFd upon complex formation with NiR. Based on HSQC signals of FdI assigned by Saitoh *et al.* (*9*), the same procedure was applied for the assignment of HSQC signals of LbFd. Sequential connectivity for the majority of amide resonances were well achieved using 2D $^{1}H–^{15}N$ HSQC, 3D HN(CO)CA, HNCACB and CACB(CO)NH measurements. Most of the amide resonance signals were detected, with the exception of three regions in the vicinity of [2Fe–2S] cluster: Try40 to Ala51, Ser65 to Phe66 and Leu78 to Val81, which were susceptible to paramagnetic effects caused by iron atoms of [2Fe–2S] cluster (Fig. 3A and B). Chemical shift values of observable amide signals (^{1}H, ^{15}N, $^{13}C_{\alpha}$ and $^{13}C_{\beta}$) are listed in Supplementary Table S3, and the $^{1}H–^{15}N$ HSQC resonance assignment of LbFd is summarized in Fig. 3A.

$^{1}H–^{15}N$ HSQC spectra of LbFd were measured in the presence of non-labelled NiR at molar ratios of 0.25, 0.5, 0.75, 1.0, 1.25 and 1.5, and a significant change in chemical shift values was observed in a set of amino acid residues upon the addition of NiR (Fig. 3C). The chemical shift perturbations of the ^{1}H and the ^{15}N nuclei of individual amides were combined according to the equation described in the 'Materials and Methods' section, and resulting values obtained at the molar ratio of 0.75 are shown in Fig. 3B.

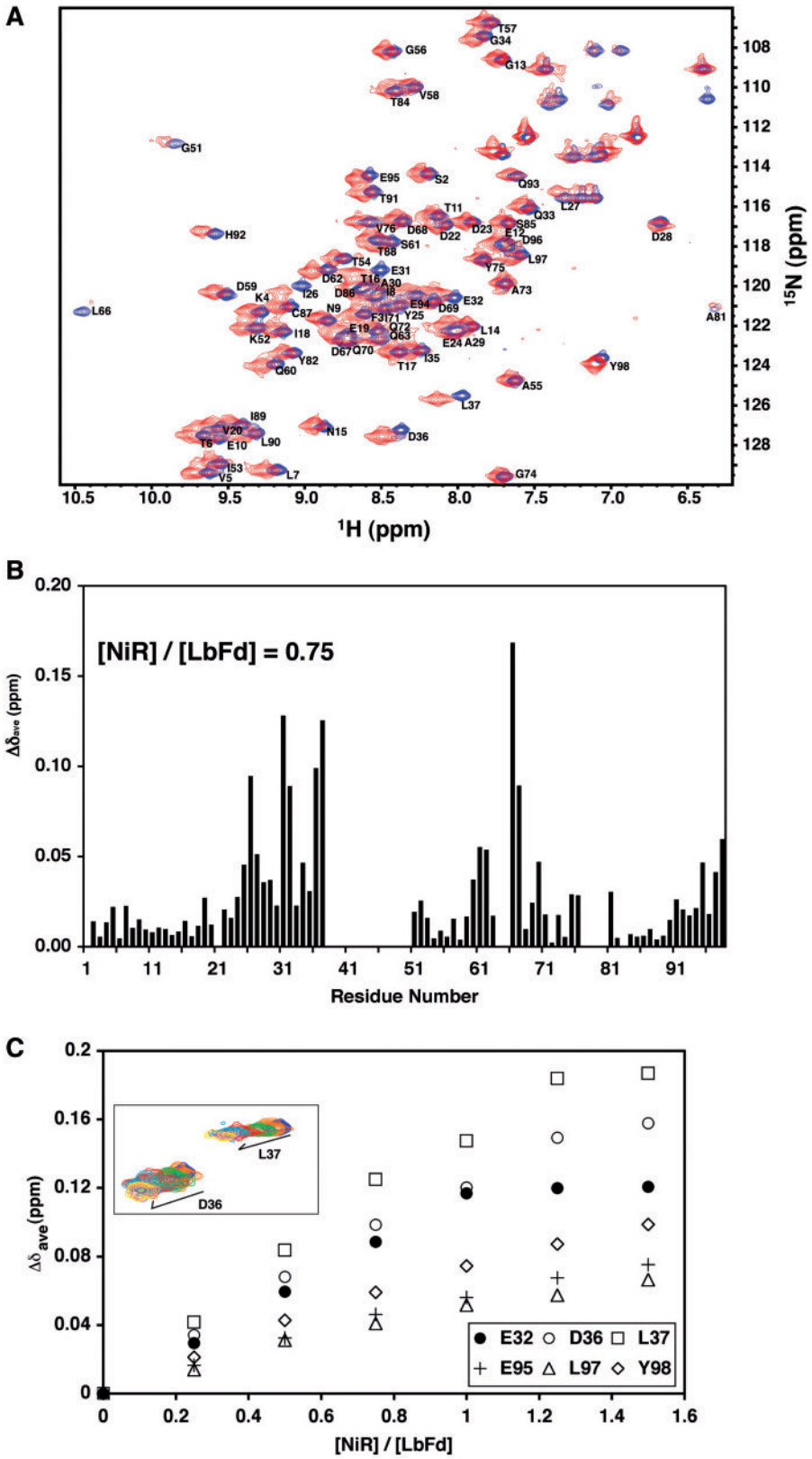

Fig. 3 NMR analysis of the interaction of LbFd with NiR. (A) ^{1}H–^{15}N HSQC spectra of [^{15}N]LbFd. Overlay of the spectra in the absence (blue) and presence (red) of NiR at a molar ratio ([NiR]/[LbFd]) of 1. Assignment of the backbone amide groups is shown in Supplementary Table S2. (B) Weighted averages ($\Delta\delta_{ave}$) of the ^{1}H and ^{15}N chemical shift changes (ppm) calculated with the equation of $\{[(\Delta\delta^{1}HN)^{2}+(0.17*\Delta\delta^{15}N)^{2}]^{1/2}\}$ on the two HSQC spectra shown in (A) are plotted against the residue number. (C) Titration curves of chemical shift changes for six representative residues of [^{15}N]LbFd. The inset is overlaid signals of two representative residues, measured under increasing molar ratio of NiR to [^{15}N]LbFd (blue: 0, orange: 0.25, green: 0.5, red: 0.75, light-blue: 1, pink: 1.25 and yellow: 1.5). Direction of chemical shift changes of LbFd is indicated by the arrow as the amount of NiR in solution increased.

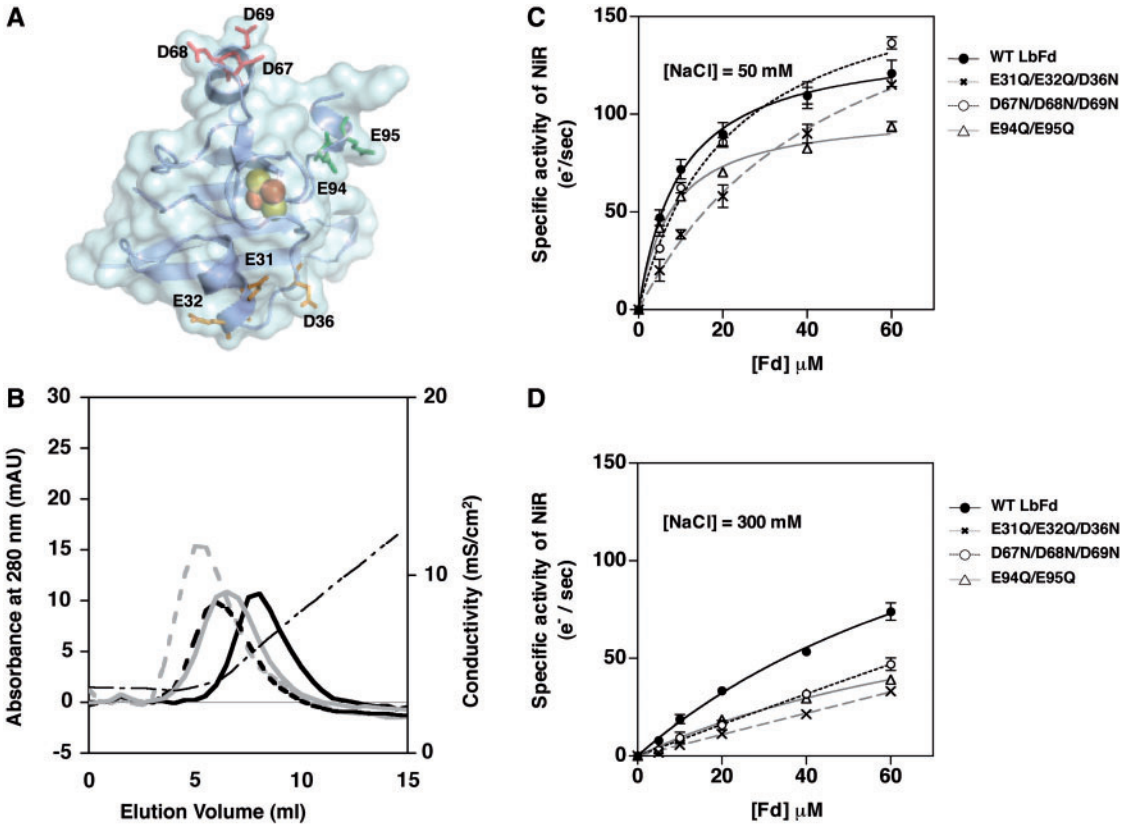

Fig. 4 Analysis of LbFd mutants with acidic regions altered. (A) Acidic residues present in three regions identified by chemical shift perturbation experiment (Fig. 3B) are shown on the 3D structure of LbFd. (B) WT and three LbFd mutants E31Q/E32Q/D36N, D67N/D68N/D69N and E94Q/E95Q were chromatographed on an NiR-immobilized Sepharose column as in Fig. 1C (black line for WT, grey dash line for E31Q/E32Q/D36N, black dash line for D67N/D68N/D69N and grey line for E94Q/E95Q). (C and D) WT and mutants of LbFd were assayed for NiR activity as in Fig. 1A and B.

The titration curves of representative residues exhibiting a significant chemical shift perturbation showed a similar profile, reaching a saturation level on increasing molar ratios of NiR (Fig. 3C). These titration experiments indicated that Fd underwent fast exchange between free and complex forms on the NMR time scale.

Based on 3D mapping of the residues that exhibited significant perturbation as shown later (Fig. 5B), three surface areas of LbFd surrounding [2Fe–2S] cluster, Tyr25 to Leu37 (α2), Ser61 to Asp62 and Leu66 to Asp67 (Loop5) and Glu95 to Tyr98 (the C-terminus), are located at the interface of the Fd/NiR complex. Interestingly, the acidic residues within these regions showed relatively large chemical shift perturbations. In addition, Ile26, which is buried inside the molecule, exhibited a significant perturbation. Most likely, this is due to an indirect effect of magnetic environmental change upon the complex formation with NiR.

Mutagenesis of acidic residues of LbFd

NMR experiments suggested three acidic regions of LbFd contribute to the protein–protein interaction with NiR. To confirm this, three mutants of LbFd: E31Q/E32Q/D36N, D67N/D68N/D69N and E94Q/E95Q were generated (Fig. 4A), and their ability to form complex with NiR was tested by NiR-affinity chromatography. The mutant LbFds eluted from a NiR-immobilized resin column at lower ionic strength than wild-type (WT), and the E31Q/E32Q/D36N mutant showed the lowest affinity for NiR among all mutants (Fig. 4B). The complex formation between LbFd and NiR was further examined by gel filtration chromatography. NiR pre-mixed with various amounts of LbFds was subjected to chromatography and the amount of LbFds co-eluted with NiR was quantified. NiR formed a complex with WT-LbFd at nearly a 1:1 ratio when an excess of Fd over NiR was present, whereas such complex formation was not seen with E31Q/E32Q/D36N or was significantly retarded with D67N/D68N/D69N and E94Q/E95Q (Supplementary Fig. S2).

These data on electrostatic interactions between LbFd mutants and NiR are correlated well with the kinetical data (Fig. 4C, D and Table 1). NiR showed significantly lower affinity for E31Q/E32Q/D36N and D67N/D68N/D69N than for WT, although E94Q/

Table I. Kinetic constants of NiR for WT and mutant LbFds.

	K_m (μM)	*k*cat ($e^- s^{-1}$)	*k*cat/K_m ($e^- s^{-1} \mu M^{-1}$)
WT LbFd	9.7 ± 1.6	138.2 ± 06.9	14.2
E31Q/E32Q/D36N	47.8 ± 9.1	203.2 ± 21.2	4.3
D67N/D68N/D69N	21.3 ± 2.4	178.3 ± 08.3	8.4
E94Q/E95Q	7.7 ± 0.9	101.4 ± 03.1	13.2

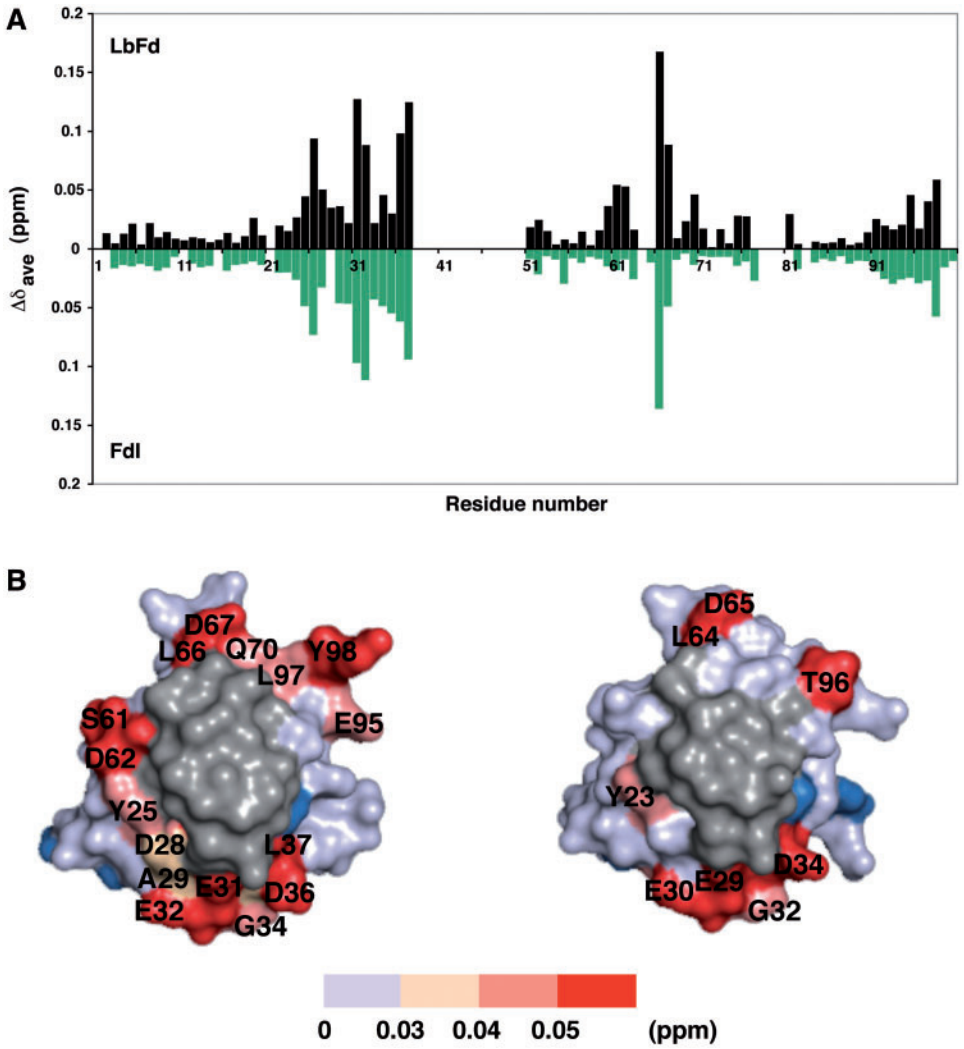

Fig. 5 Comparison of the interaction with NiR between LbFd and FdI. (A) Comparison of backbone amide resonance changes of [^{15}N]LbFd (black) and [^{15}N]FdI (green) upon complex with NiR. (B) Mapping of the chemical shift changes on the 3D structures of LbFd (left) and FdI (right). Chemical shift change of each residue is coloured as scale bar shown. Residues near [2Fe–2S] cluster, whose chemical shift data are not available due to the paramagnetic effect of the iron, are shown in grey. The unassigned amide proton of proline residues are coloured in blue.

E95Q retained an affinity comparable with WT (Fig. 4C and Table 1). In the presence of 300 mM NaCl, all three mutant LbFds exhibited a greater decrease in activity than WT (Fig. 4D).

Comparison of NiR-interacting sites of FdI and LbFd

Although FdI shows a high similarity to LbFd in overall molecular configuration, NiR shows lower activity for FdI than LbFd. We hypothesized that the interaction mode of these two Fds with NiR is somehow different. To explore the reason for distinctive characteristics of two Fds, NMR chemical shift perturbation experiments using FdI were carried out under the same conditions as LbFd. As shown in Fig. 5A and B, there was no remarkable difference between two Fds in the pattern of the chemical shift perturbation or in the distribution of the residues with large resonance changes on their 3D structures. There are a few residues unique to each Fd on the side of NiR interaction; Ser43, Ser46, Try63, His78, Thr96, Gly97 and Ala98 in FdI, and Ala45, Thr48, Phe65, Val80 and Tyr98 in LbFd. We superimposed the overall structure of two Fds and calculated RMSD in the backbone and side-chain of 96 residues of LbFd (Supplementary Fig. S3). Two regions are largely shifted in the backbone due to the insertion of residues 11 and 15 of LbFd and due to the addition of residues 97 and 98 of FdI. Large shift is also observed in the side-chains of residues 20–38, 50–66 and 80–96 of FdI which correspond to residues 22–40, 52–68 and 82–98 of LbFd, respectively, although most of these residues are identical or similar between two Fds. We have checked an influence of crystal packing on the topological difference of the corresponding side chains of two Fds on their 3D structures and considered that the contribution of the packing effect on the large RMSD values of the side-chain between two Fds is marginal, if any.

To investigate whether these subtle structural alterations are attributed to the functional differences of two Fds, all the unique amino acids of each Fd listed above were interchanged to make FdI-type LbFd and LbFd-type FdI (Supplementary Fig. S3A) and these

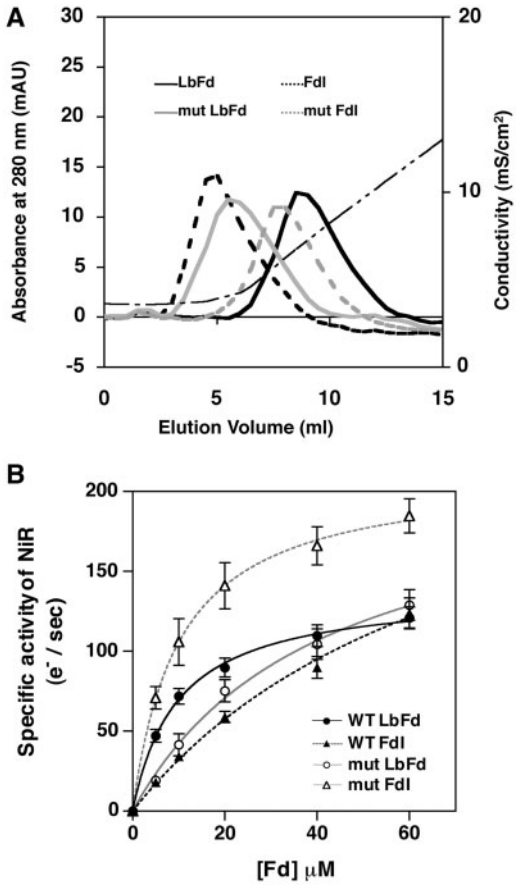

Fig. 6 NiR activity and binding assay of LbFd, FdI and their interchanged mutants. (A) Fd was chromatographed on an NiR-immobilized Sepharose column as in Fig. 1C. Two mutants, FdI-type LbFd mutant and LbFd-type FdI mutant are abbreviated as mut LbFd and mut FdI, respectively. (B) WT and mutant Fds were assayed for NiR activity as in Fig. 1A.

mutant Fds were characterized in comparison with the original molecules. As shown in Fig. 6A and B, the ability of FdI to bind to NiR resin and to donate electron to NiR was clearly increased to the level of LbFd by introduction of LbFd-type mutation and the ability of LbFd were conversely decreased by introduction of the opposite mutation.

Discussion

In this study, we applied NMR spectroscopy to investigate the protein–protein interaction between Fd and NiR from cyanobacteria. Based on the chemical shift perturbations of $^{1}H-^{15}N$ HSQC spectra of [^{15}N]Fd upon interaction with NiR, three regions of LbFd with negative surface potential, Tyr25 to Leu37, Ser61 to Gln70 and Glu95 to Leu97, were considered to be major sites involved in the interaction with NiR. This result was consistent with the data obtained by site-directed mutation of acidic residues located in the three regions, giving evidence that the Fd/NiR complex is stabilized through electrostatic force. As E31Q/E32Q/D36N showed the largest decrease among the three mutants in the ability of the electron donor to NiR and in the physical interaction with NiR, we propose these negatively charged residues in Fd have a major contribution to the electrostatic interaction most probably with positively charged residues in NiR.

An *in silico* docking model of the complex structure of spinach Fd and NiR was reported (*35*). In this model, Ser43, Asp60 and Glu93 in spinach Fd, which correspond to Ala45, Asp62 and Glu95 in LbFd, are proposed to be involved in stabilizing the Fd/NiR complex through salt bridge and hydrogen bond with counterpart residues in NiR. In consistent with this, our NMR data showed that Asp62 and Glu95 are the residues with notable shift perturbation. However, Glu31, Glu32 and Asp36, which are mainly involved in the interaction in the cyanobacterial Fd/NiR complex, do not seem to be located at the interface of the spinach Fd/NiR complex in the model structure. Interaction sites of the Fd/NiR complex might differ at least partly between cyanobacteria and spinach. Additional works such as crystallographic analysis of the Fd/NiR complex would be necessary to address this hypothesis.

We have previously studied the interaction of Fd with two other Fd-dependent enzymes, FNR and SiR, by NMR spectroscopy (*9*). A clear difference was observed between the chemical shift perturbations of Fd upon complex with NiR and FNR. Fd seems to bind to these enzymes in a different way. No significant difference was observed between the Fd/NiR and Fd/SiR complexes, since SiR is an enzyme structurally homologous with NiR.

In the present study, maize Fd was found to have much weaker affinity with NiR than cyanobacterial Fd, although maize Fd has an ability to support NiR activity with efficiency comparable with or even higher than cyanobacterial Fd in the assay with Fd concentration >50 μM (Fig. 1A). This nature of maize Fd could not be explained only by a weaker electrostatic interaction of the Fd/NiR complex than cyanobacterial Fd, since distribution of acidic residues on its primary structure and electrostatic surface potential are well conserved between two Fds. Actually, the chemical shift perturbations of two Fds with NiR determined by NMR spectroscopy are quite similar (Fig. 5B). Seven residues in FdI, Ser43, Ser46, Tyr63, His78, Thr96, Gly97 and Ala98, located on the interface side of the Fd/NiR complex, are different from the corresponding residues in cyanobacterial Fd, Ala45, Thr48, Phe65, Val80, Tyr98 and deletions at position 99 and 100. A mutant of maize Fd with these residues substituted as in cyanobacterial Fd showed a higher affinity comparable with cyanobacterial Fd. Such a gain-of-function result strongly indicates that the non-charged residues contribute significantly to the stabilization of the Fd/NiR complex. In the Fd/FNR complex, hydrophobic force in the interface of the two proteins was shown to be thermodynamically important for the stabilization of the complex (*2*, *36*).

Most of the non-charged residues listed above are separately conserved both in cyanobacterial and plant Fds (*36*, *37*). Thus, two evolutionary divergent Fds may differentiate in terms of a fine mechanism of the molecular recognition for Fd-dependent enzymes. It should be mentioned that much is remaining

unsolved for *in vivo* control mechanisms involved in distributing photosynthetic reducing power to various redox metabolisms. A large body of data so far obtained from biochemical, physicochemical and structure biological studies give the general thought that an electrostatically stabilized complex between Fd and Fd-dependent enzymes plays a major role in such electron partitioning. This study adds a new aspect that hydrophobic and/or van der Waals interaction should be taken into consideration to understand such mechanisms.

SUPPLEMENTARY DATA

Supplementary Data are available at *JB* Online.

Conflict of interest
None declared.

References

1. Hanke, G.T., Kimata-Ariga, Y., Taniguchi, I., and Hase, T. (2004) A post genomic characterization of Arabidopsis ferredoxins. *Plant Physiol.* **134**, 255–264
2. Kurisu, G., Kusunoki, M., Katoh, E., Yamazaki, T., Teshima, K., Onda, Y., Kimata-Ariga, Y., and Hase, T. (2001) Structure of the electron transfer complex between ferredoxin and ferredoxin-NADP(+) reductase. *Nat. Struct. Biol.* **8**, 117–121
3. Fukuyama, K. (2004) Structure and function of plant-type ferredoxins. *Photosynth. Res.* **81**, 289–301
4. Binda, C., Coda, A., Aliverti, A., Zanetti, G., and Mattevi, A. (1998) Structure of the mutant E92K of [2Fe-2S] ferredoxin I from *Spinacia oleracea* at 1.7 Å resolution. *Acta Crystallogr. D Biol. Crystallogr.* **54**, 1353–1358
5. Dai, S., Friemann, R., Glauser, D.A., Bourquin, F., Manieri, W., Schurmann, P., and Eklund, H. (2007) Structural snapshots along the reaction pathway of ferredoxin-thioredoxin reductase. *Nature* **448**, 92–96
6. Hurley, J.K., Morales, R., Martinez-Julvez, M., Brodie, T.B., Medina, M., Gomez-Moreno, C., and Tollin, G. (2002) Structure-function relationships in *Anabaena* ferredoxin/ferredoxin: NADP(+) reductase electron transfer: insights from site-directed mutagenesis, transient absorption spectroscopy and X-ray crystallography. *Biochim. Biophys. Acta* **1554**, 5–21
7. Hase, T., Schurmann, P., and Knaff, D.B. (2006) The interaction of ferredoxin with ferredoxin-dependent enzymes in *Advances in Photosynthesis and Respiration* (Golbeck, J.H., ed.) Vol. 24, pp. 477–498, Springer, Dordrecht, The Netherlands
8. Morales, R., Kachalova, G., Vellieux, F., Charon, M.-H., and Frey, M. (2000) Crystallographic studies of the interaction between the ferredoxin-NADP+ reductase and ferredoxin from the cyanobacterium *Anabaena*: looking for the elusive ferredoxin molecule. *Acta Crystallogr D Biol Crystallogr.* **56**, 1408–1412
9. Saitoh, T., Ikegami, T., Nakayama, M., Teshima, K., Akutsu, H., and Hase, T. (2006) NMR study of the electron transfer complex of plant ferredoxin and sulfite reductase: mapping the interaction sites of ferredoxin. *J. Biol. Chem.* **281**, 10482–10488
10. Xu, X., Kim, S.K., Schurmann, P., Hirasawa, M., Tripathy, J.N., Smith, J., Knaff, D.B., and Ubbink, M. (2006) Ferredoxin/ferredoxin-thioredoxin reductase complex: complete NMR mapping of the interaction site on ferredoxin by gallium substitution. *FEBS Lett.* **580**, 6714–6720
11. Onda, Y., Matsumura, T., Kimata-Ariga, Y., Sakakibara, H., Sugiyama, T., and Hase, T. (2000) Differential interaction of maize root ferredoxin: NADP(+) oxidoreductase with photosynthetic and non-photosynthetic ferredoxin isoproteins. *Plant Physiol.* **123**, 1037–1045
12. Akashi, T., Matsumura, T., Ideguchi, T., Iwakiri, K., Kawakatsu, T., Taniguchi, I., and Hase, T. (1999) Comparison of the electrostatic binding sites on the surface of ferredoxin for two ferredoxin-dependent enzymes, ferredoxin-NADP(+) reductase and sulfite reductase. *J. Biol. Chem.* **274**, 29399–29405
13. Mikami, B. and Ida, S. (1989) Spinach ferredoxin-nitrite reductase: characterization of catalytic activity and interaction of the enzyme with substrates. *J. Biochem.* **105**, 47–50
14. Kuznetsova, S., Knaff, D.B., Hirasawa, M., Lagoutte, B., and Setif, P. (2004) Mechanism of spinach chloroplast ferredoxin-dependent nitrite reductase: spectroscopic evidence for intermediate states. *Biochemistry* **43**, 510–517
15. Kuznetsova, S., Knaff, D.B., Hirasawa, M., Setif, P., and Mattioli, T.A. (2004) Reactions of spinach nitrite reductase with its substrate, nitrite, and a putative intermediate, hydroxylamine. *Biochemistry* **43**, 10765–10774
16. Hirasawa, M., Nakayama, M., Hase, T., and Knaff, D.B. (2004) Oxidation-reduction properties of maize ferredoxin: sulfite oxidoreductase. *Biochim. Biophys. Acta* **1608**, 140–148
17. Swamy, U., Wang, M., Tripathy, J.N., Kim, S.K., Hirasawa, M., Knaff, D.B., and Allen, J.P. (2005) Structure of spinach nitrite reductase: implications for multi-electron reactions by the iron-sulfur:siroheme cofactor. *Biochemistry* **44**, 16054–16063
18. Sekine, K., Sakakibara, Y., Hase, T., and Sato, N. (2009) A novel variant of ferredoxin-dependent sulfite reductase having preferred substrate specificity for nitrite in the unicellular red alga *Cyanidioschyzon merolae*. *Biochem. J.* **423**, 91–98
19. Hirasawa, M., Tripathy, J.N., Somasundaram, R., Johnson, M.K., Bhalla, M., Allen, J.P., and Knaff, D.B. (2009) The interaction of spinach nitrite reductase with ferredoxin: a site-directed mutation study. *Mol. Plant* **2**, 407–415
20. Kimata-Ariga, Y., Matsumura, T., Kada, S., Fujimoto, H., Fujita, Y., Endo, T., Mano, J., Sato, F., and Hase, T. (2000) Differential electron flow around photosystem I by two C-4-photosynthetic-cell-specific ferredoxins. *EMBO J.* **19**, 5041–5050
21. Hase, T., Kimata, Y., Yonekura, K., Matsumura, T., and Sakakibara, H. (1991) Molecular-cloning and differential expression of the maize ferredoxin gene family. *Plant Physiol.* **96**, 77–83
22. Matsumura, T., Kimata-Ariga, Y., Sakakibara, H., Sugiyama, T., Murata, H., Takao, T., Shimonishi, Y., and Hase, T. (1999) Complementary DNA cloning and characterization of ferredoxin localized in bundle-sheath cells of maize leaves. *Plant Physiol.* **119**, 481–488
23. Arizmendi, J.M. and Serra, J.L. (1990) Purification and some properties of the nitrite reductase from the cyanobacterium *Phormidium laminosum*. *Biochim. Biophys. Acta* **1040**, 237–244

24. Yonekura-Sakakibara, K., Onda, Y., Ashikari, T., Tanaka, Y., Kusumi, T., and Hase, T. (2000) Analysis of reductant supply system for ferredoxin-dependent sulfite reductase in photosynthetic and non-photosynthetic organs of maize. *Plant Physiol.* **122**, 887–894
25. Vagin, A. and Teplyakov, A. (1997) MOLREP: an automated program for molecular replacement. *J. Appl. Cryst.* **30**, 1022–1025
26. Emsley, P., Lohkamp, B., Scott, W.G., and Cowtan, K. (2010) Features and development of Coot. *Acta Crystallogr. D Biol. Crystallogr.* **66**, 486–501
27. Laskowski, R.A., MacArthur, M.W., Moss, D.S., and Thornton, J.M. (1993) PROCHECK: a program to check the stereochemical quality of protein structures. *J. Appl. Cryst.* **26**, 283–291
28. Thompson, J.D., Higgins, D.G., and Gibson, T.J. (1994) CLUSTAL W: improving the sensitivity of progressive multiple sequence alignment through sequence weighting, position-specific gap penalties and weight matrix choice. *Nucleic Acids Res.* **22**, 4673–4680
29. Dolinsky, T.J., Nielsen, J.E., McCammon, J.A., and Baker, N.A. (2004) PDB2PQR: an automated pipeline for the setup of Poisson-Boltzmann electrostatics calculations. *Nucleic Acids Res.* **32**, W665–W667
30. Kaiser, W.M., Schroppelmeier, G., and Wirth, E. (1986) Enzyme-activities in an artificial stroma medium - an experimental-model for studying effects of dehydration on photosynthesis. *Planta* **167**, 292–299
31. Zuiderweg, E.R.P. (2002) Mapping protein-protein interactions in solution by NMR Spectroscopy. *Biochemistry* **41**, 1–7
32. Delaglio, F., Grzesiek, S., Vuister, G.W., Zhu, G., Pfeifer, J., and Bax, A. (1995) Nmrpipe - a multidimensional spectral processing system based on UNIX pipes. *J. Biomol. NMR* **6**, 277–293
33. Goddard, T.D. and Kneller, D.G. (1999) *SPARKY 3*, University of California, San Francisco
34. Bailey, S. (1994) The ccp4 suite - programs for protein crystallography. *Acta Crystallogr. D Biol. Crystallogr.* **50**, 760–763
35. Hirasawa, M., Tripathy, J.N., Somasundaram, R., Johnson, M.K., Bhalla, M., Allen, J.P., and Knaff, D.B. (2009) The interaction of spinach nitrite reductase with ferredoxin: a site-directed mutation study. *Mol. Plant* **2**, 407–415
36. Jelesarov, I. and Bosshard, HR. (1994) Thermodynamics of ferredoxin binding to ferredoxin:$NADPH^+$ reductase and the role of water at the complex interface. *Biochemistry* **33**, 13321–13328
37. Kameda, H., Hirabayashi, K., Wada, K., and Fukuyama, K. (2011) Mapping of protein-protein interaction sites in the plant-type [2Fe-2S] ferredoxin. *PLos One* **6**, e21947